Measurement and Characterization of HEMT Dynamics

Anthony E. Parker, *Senior Member, IEEE*, and James Grantley Rathmell, *Member, IEEE*

***Abstract*—The variation of high electron-mobility transistor (HEMT) large-signal behavior with a change in operating condition is examined with a view to understanding the dynamics involved and developing a modeling strategy. The observed variation exhibits the dynamics of thermal, impact ionization, and trapping effects. A novel measurement of drain characteristic transients gives time-evolution information that clearly shows these as separate quantifiable phenomena with significant dependence on initial operating conditions. A drain–current model that describes high-frequency characteristics with pinchoff, gain, and drain feedback parameters is adapted to describe the variation of the characteristics with changing operating conditions. The results reported give insight and grounding for simulation of HEMT circuits.**

***Index Terms*—HEMTs, high-speed devices, impact ionization, kink effect, pulsed characterization.**

I. Introduction

Apart from providing efficient and accurate simulation of circuits, models that describe high electron-mobility transistors (HEMTs) should be applicable to frequencies ranging from dc to microwave, cover a wide range of operating conditions, and should contribute to an understanding of the operation of the device. For any fixed operating condition, devices give an instantaneous response to high-frequency signals, which is well described by either small- or large-signal models. However, the response to microwave signals exhibits a significant variation with the operating condition that is a serious simulation problem for many applications in which the operating point depends on the signal conditions. For example, particular forms of asymmetric distortion and various modulation schemes give rise to changing average or dc conditions of an amplifier. Other applications that will suffer are those that deliberately vary operating conditions or that involve frequencies comparable to that of the operating-condition dependency. The dependency needs to be quantified and incorporated in the device models.

Steady-state RF measurements provide good small-signal characterization of high-frequency devices that is applicable to one operating condition—the operating condition used for the measurement. Models fitted to steady-state measurements describe S-parameters, intermodulation characteristics, or large-signal parameters at the particular operating point at which the device is to be used. Isodynamic pulsed measurements provide a good characterization of the large-signal response to microwave signals that is also applicable to one operating condition—that of the measurement [1], [2]. If the operating point is changed, the characteristics are found to deviate and a new measurement and model is required. Alternatively, a universal model would incorporate the dynamics of phenomena involved in the dependency on operating conditions. A characterization strategy that provides this information is required for such a model.

Phenomena, collectively called *dispersion effects*, are responsible for the operating point dependency of device characteristics. Although the classification of dispersion effects into thermal, electron trapping, and other mechanisms is common, the characterization and modeling of their dynamics is still a sought-after goal [3]–[6]. Thermal and charge effects are observed in steady-state dc and RF measurements, but their dynamic behavior and the existence of other dispersion effects cannot be inferred uniquely from the steady-state data [7]. The characterization strategy required by a universal model is one that can quantify these dispersion effects.

The following sections report a study of dispersion dynamics based on the time-evolution of HEMTs from their pulsed-*I/V* characteristics to their dc characteristics. This gives a clear view of the dynamics of the dispersion effects in the HEMTs. Section II discusses issues in the pulsed measurement of high-speed devices and the transition from instantaneous to dc characteristics. This transition exhibits clearly separable and quantifiable thermal, impact ionization, and trapping effects. The initial operating condition has a significant influence on this transition, which is explored in a discussion of observations in Section III.

Section IV discusses the adaption of a drain–current model to describe the variation of the characteristics with changing operating conditions. To do this, the dynamics of the dispersion effects are incorporated. The resulting model tracks changes in operating conditions and is able to predict circuit phenomena such as gate–lag and drain overshoot.

II. Time/Pulse Characterization

Pulse measurements facilitate examination of high-frequency characteristics as a function of operating point. An isodynamic pulse measurement maintains a constant operating condition and then applies a varying pulse stimulus, such that the characteristics are measured at a rate faster than the dispersion effects.

Manuscript received February 27, 2001. This work was supported by the Australian Research Council, by the Commonwealth Scientific and Industrial Research Organization Division of Telecommunications and Industrial Physics, and by Agilent Technologies.

A. E. Parker is with the Department of Electronics, Macquarie University, Sydney 2109, N.S.W., Australia (e-mail: tonyp@ieee.org).

J. G. Rathmell is with the School of Electrical and Information Engineering, The University of Sydney, Sydney 2006, N.S.W., Australia (e-mail: jimr@ee.usyd.edu.au).

Publisher Item Identifier S 0018-9480(01)09371-1.

Recent availability of pulsed-bias and pulsed-RF measurement equipment [1], [2] has given a comprehensive picture of the operating-point dependency through repeated measurement over various operating points, such as that of a preliminary study carried out on an HEMT [8]. It has been established that the high-frequency characteristics are significantly influenced by the average operating condition and are very different from the dc characteristics. Fig. 1 illustrates this with the pulsed-*I/V* characteristics of an HEMT at different operating points, together with the dc curve. The different instantaneous characteristics of an HEMT must be considered as a function of operating point and of signal potentials with respect to the operating point.

For the particular pulsewidth (100 ns) employed in Fig. 1, there is an obvious dependency on initial operating condition that features a *kink* effect. There is distinctly different behavior on either side of the kink. Thermal-related reduction in current is a dominant property of the dc characteristics. The time of occurrence of the thermal effect, the change in the kink, and the existence of other dispersion effects remains unobserved. The issue that arises is that of what constitutes a change in the operating condition and what processes occur during the change. To address this, the transition from the pulsed characteristics to the dc characteristics was measured. This gives a time evolution from the instantaneous characteristics to the dc characteristics.

For this study, the time evolution of HEMT characteristics was measured from several initial operating conditions. Each point in the *I/V* characteristic was observed from the time of a step change in the operating condition until it settled to a new dc value. Each point in the pulsed characteristics of Fig. 1 is the start of a transition to a new operating point from the initial condition before the pulse. If the point is visited briefly followed by a return to the initial condition, as is the case in Fig. 1, then the operating point is not changed. However, if the pulsewidth is extended, then the HEMT's drain current will eventually settle to that of the corresponding point in the dc characteristics. During the transition, the cumulative effects of the dispersion are observable.

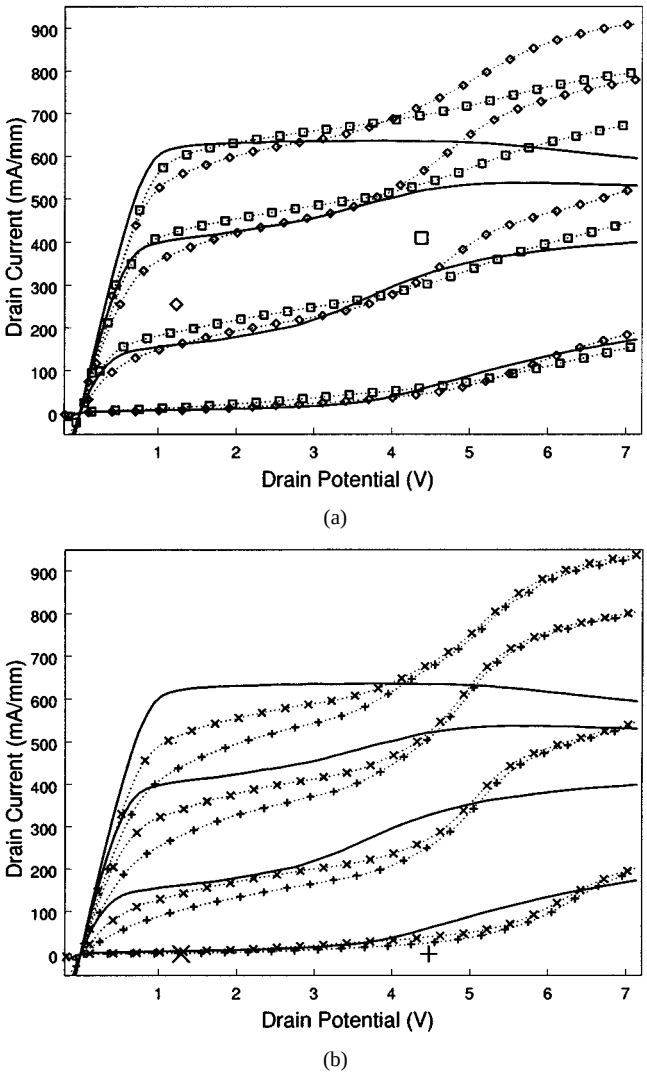

Fig. 1. DC and pulsed characteristics at 100 ns for four initial operating conditions with v_{GS} at -1.5, -1.0, -0.5, and 0.0 V as the parameter. The two sets of pulse data cover the same terminal potentials as the dc data (—). Shown is pulse data (◇) from initial point (◇) at $V_{GS} = -0.75$ V and $V_{DS} = 1.2$ V, data (□) from initial point (□) at $V_{GS} = -0.75$ V and $V_{DS} = 4.2$ V, data (×) from initial point (×) at $V_{GS} = -2.0$ V and $V_{DS} = 1.2$ V, and data (+) from initial point (+) at $V_{GS} = -2.0$ V and $V_{DS} = 4.2$ V.

A. Time-Evolution Measurement

An enhanced arbitrary-pulse semiconductor parameter analyzer[1] was used to measure the time evolution of an HEMT. The stability and accuracy of the measurement was of particular importance for this study. Due to the common-source configuration of the sample devices and the need to have a low driver resistance, current was measured using a floating differential amplifier that detects the voltage across a sense resistor through which the drain current was passed. Common-mode voltage gain of the current sensor increases with frequency, but was reduced by floating of the amplifier's power supply. The current measurement was tested and found to be stable and accurate from less than 100 ns to over 100 s.

In pulsing to each desired stimulus point, the effect of drift and transit responses of the voltage amplifiers that drive the device is avoided by sampling voltages directly at the device. Several points in the vicinity of a desired point in the characteristic were measured and the current at that point was determined by software interpolation. This was repeated for all points in the final characteristics and at each time point. The rise time of the stimulus was less than 50 ns. Drain current and terminal voltages were sampled at 64 points distributed logarithmically from 100 ns to 100 ms. A display of current on a logarithmic time scale shows transitions over many decades of time more clearly.

B. Time-Evolution Data

The interpolated data from a time-evolution measurement gives, for an initial operating condition, a set of *I/V* characteristics at time points from 100 ns to 100 ms. This is shown for four initial operating points in Fig. 2(a)–(d). This figure shows the initial condition (drain current and potential) before the transition as a solid line—constant in time. Each surface gives, for a constant gate potential, the drain current versus

[1]Arbitrary pulse semiconductor parameter analyzer, Sydney, Australia, 2001. [Online]. Available: http://www.elec.mq.edu.au/cnerf/

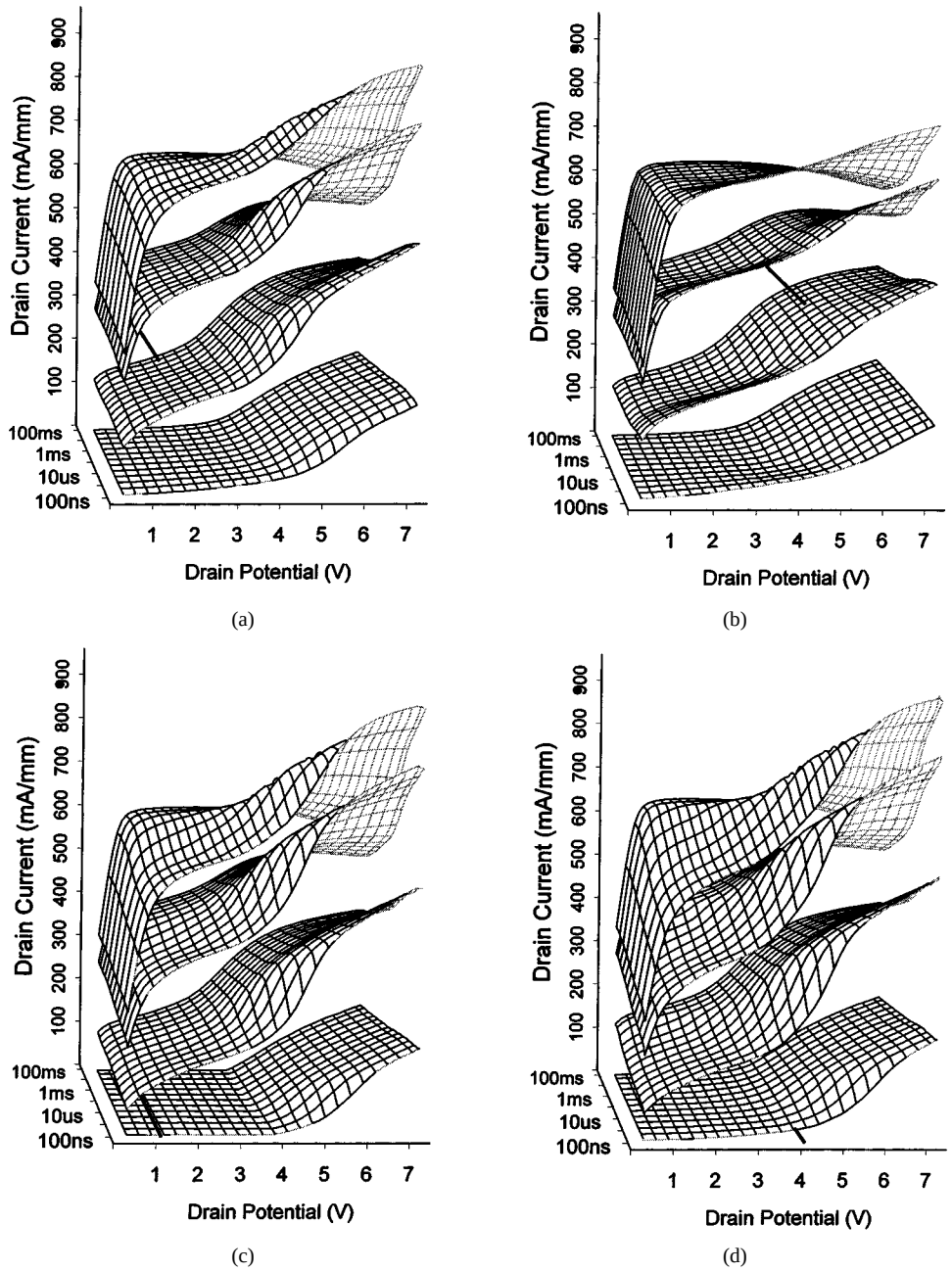

Fig. 2. Transient drain characteristics as a function of time after a step change from the initial condition shown by solid lines (—). Each graph shows surfaces of drain current with v_{GS} at -1.5, -1.0, -0.5, and 0.0 V as the parameter. (a) From $V_{GS} = -0.75$ V, $V_{DS} = 1.2$ V. (b) From $V_{GS} = -0.75$ V, $V_{DS} = 4.2$ V. (c) From $V_{GS} = -2.0$ V, $V_{DS} = 1.2$ V. (d) From $V_{GS} = -2.0$ V, $V_{DS} = 4.2$ V.

time and drain potential. The rear edge, at 100 ms, is the dc characteristic shown in Fig. 1. The front edge, at 100 ns, is the pulse characteristics shown in Fig. 1.

When interpreting this data, it is better to consider each point in the characteristics in isolation. That is, the transition is from the initial condition, shown by a solid line in Fig. 2, at zero time to a point on the front edge of a current surface. As time progresses, the current then follows a line of constant drain potential toward its final dc value. Depending on which point in the characteristic is considered, the time evolution passes through various changes in current.

Fig. 2(a)–(d) clearly demonstrates that it is important to attach a time parameter to the pulse measurements. The time from application of a particular pulse stimulus is an important aspect of the measurement.

III. Observations

Several phenomena are observed and can be separated and quantified by studying the data in Fig. 2. The effect known as *drain overshoot* is observed at the high-drain-potential low-time corner of the high-current surface. That is, when a step transition to a high-power point from a moderate operating point occurs, the drain current is observed to rise quickly and then settle to a smaller value. The effect known as *gate lag* is observed after a transition from pinchoff to moderate drain current and potential.

That is, when turning on the device, the current rises rapidly and, then, after several microseconds, rises further. The phenomena contributing to these effects are explored in the following subsections.

A. Thermal Dispersion

An important effect observed in the characteristics of the relatively large device shown in Figs. 1 and 2 is self-heating due to the power dissipation at the operating points. Being related to power, this form of dispersion is dominant at high currents and high drain potential. It is responsible for the apparent negative conductance in the dc characteristics and contributes to the reduction in drain current. This can be described by the following simple thermal model:

$$i_{DS} = i_{D(T_0)}\left(1 - \delta \overline{P}\right) \tag{1}$$

where $i_{D(T_o)}$ is the *isothermal current* that would flow if there was no temperature-related variation due to the average power dissipation $\overline{P}$. This is derived by assuming that the instantaneous drain current i_{DS} is a linear function of temperature rise ΔT[K] with thermal coefficient $\lambda[K^{-1}]$, $i_{DS} = i_{D(T_o)}(1 - \lambda \Delta T)$; and that the temperature rise is the product of thermal resistance R_T[K/W] and power dissipation $\Delta T = R_T \overline{P}$. A *thermal resistance-temperature coefficient* parameter $\delta = \lambda R_T[W^{-1}]$ is used [8].

The isothermal characteristics can be determined from the data shown in Fig. 1 using (1). Note that, for dc measurements, each point is at its own bias, thus, $\overline{P} = i_{DS} v_{DS}$. For isothermal pulse measurements, the average power dissipation is that of the initial operating point $\overline{P} = I_{DS} V_{DS}$. However, there is some initial junction heating prior to the first pulse sample at 100 ns. To account for this, the bias power can be estimated from a weighted average of the power dissipation of the initial point and of the pulse $\overline{P} = \kappa I_{DS} V_{DS} + (1 - \kappa) i_{DS} v_{DS}$.

The resulting isothermal characteristics for $\delta = 0.1$ [mm/W] and $\kappa = 0.95$ are shown in Fig. 3. This figure shows that, for each point at potentials greater than that of the kink effect, the currents in the characteristics have converged near a common value for that point. This implies that dispersion in this high-drain-potential region is dominated by self-heating, as described by (1). This is especially true at intermediate drain currents. The differences in the isothermal curves near pinchoff (low drain current) could be partly attributed to temperature dependence of the pinchoff potential that has not been accounted for. The significant variation between the pulse and dc curves in the other regions can be attributed to impact ionization and trapping effects.

B. Impact Ionization

The dominant nonthermal dispersion effect is the *kink* in the characteristics of Figs. 1–3 . There is a critical drain potential below which there is a significant time constant associated with the time evolution of the current from the initial 100 ns of the pulse to the dc value. Careful examination of Fig. 2 reveals that this time constant varies considerable with drain potential. The surfaces in Fig. 2(d) display this most clearly. For example, following a line of constant drain potential across the

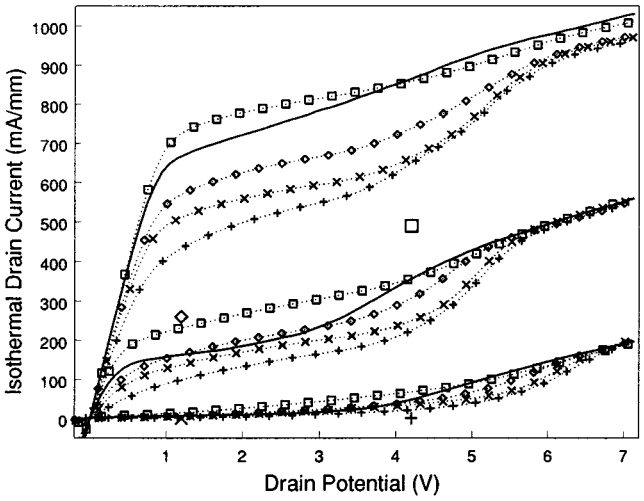

Fig. 3. DC and pulsed characteristics of Fig. 1 transformed to isothermal conditions with v_{GS} at -1.5, -1.0, and 0.0 V as the parameter. The symbols for each curve and initial operating conditions are identical to those of Fig. 1. Note that the curves for $v_{GS} = -0.5$ V have been omitted for clarity.

$v_{GS} = -1.0$ V surface shows the variation of current with time. A line at a low drain potential near 1.5 V is constant for the first few divisions and then, at about 1 ms, a transition from the initial pulse current to the dc value occurs. At drain potentials near 4 V, the transition occurs during the first few divisions, i.e., at about 1 μs. At higher potentials, it is reasonable to assume that the transition occurs much earlier than the 100-ns edge of the surfaces shown.

Considerable progress has been made in attributing the kink effect to aspects of impact ionization [6], [9], [10]. When an impact ionization current is established in the channel, there is some tunneling of charge from this current to traps sites outside the channel region [11]. The potential built up in these trap sites influences the channel current in the same way as the gate potential does. The transconductance of the device amplifies the trap potential to give an additional current contribution that is usually greater than the contribution from impact ionization alone. Both of these current contributions are present in the dc characteristics, whereas only impact ionization current contributes to the initial value of the pulse characteristics before the traps are affected.

The traps are occupied at a rate proportional to the probability that charge carriers will migrate to or from the trap sites. This rate is proportional to the number of carriers available, which are those in the impact ionization current. This current is described by [10]

$$i_I = A I_{DS} \exp\left(\frac{-B}{V_{DS} - V_{DS_{\text{sat}}}}\right) \tag{2}$$

where A and B vary between HEMT processes and bias conditions. The higher this current is, the faster the traps can fill. Thus, the important feature of dispersion caused by impact ionization is that the time constant for the buildup of trap potentials is inversely proportional to the impact ionization current. This predicts the long time constants observed at low drain potential in Fig. 2. Fig. 2(c) and (d), which start from a zero current condition, best displays this. The drain current undergoes a rise at

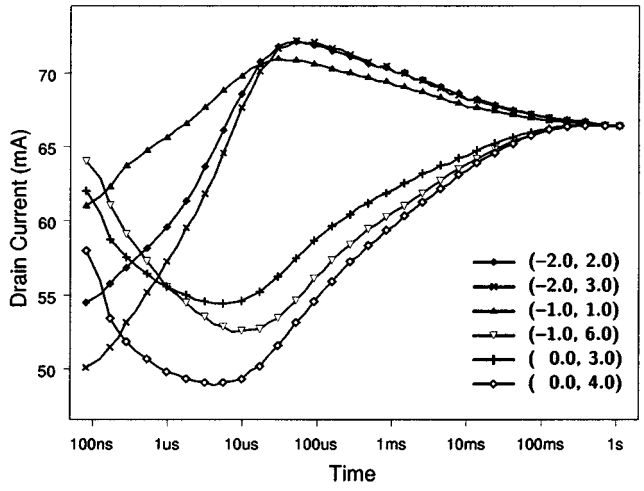

Fig. 4. Drain current as a function of time, after a step change from different initial operating conditions, to the point $(V_{GS}, V_{DS}) = (-1\text{V}, 3\text{V})$. The initial condition for each curve is indicated by the (V_{GS}, V_{DS}) voltage pairs listed in the inset legend.

a time that is inversely related to the drain voltage. For Fig. 2(a) and (b), the effect of impact ionization is far less pronounced, as the traps involved are mostly filled at the initial operating condition.

C. Transient Response

Describing the transient behavior of HEMTs in simple terms such as drain overshoot and gate lag overlooks the simultaneous action of more than one dispersion effect. Thermal effects can produce drain overshoot, and impact ionization effects can produce gate lag. However, as seen in the time-domain profile of Fig. 4, both effects occur in the transients. This figure shows (as a function of time) drain current after pulsing to a particular point from six initial operating points. The point pulsed to is $V_{GS} = -1V$, $V_{DS} = 3V$. The range of initial points was chosen to give changes with constant V_{GS}, constant V_{DS}, and constant V_{DG}.

The lower three transients in Fig. 4 are from initial currents and power dissipations that are higher than the final point. The transients exhibit an initial reduction in current due to a reduction in impact ionization, followed by an increase in current as the device cools down.

The upper three transients in Fig. 4 are from initial conditions with currents and power dissipations lower than the final point. The transients exhibit an initial increase in current due to an increase in impact ionization, followed by an decrease in current as the device heats up.

IV. Dispersion Modeling

A model of the large-signal dynamic behavior of an HEMT is proposed in light of the observations above. The drain current is described in terms of instantaneous terminal potentials v_{GS} and v_{GD}, the time-averaged terminal potentials $\overline{V_{GS}}$ and $\overline{V_{GD}}$, and time-averaged power dissipation $\overline{I_{DS}V_{DS}}$ (five variables) in a similar fashion as the previous rate-dependent MESFET model of [12]. Self-heating is implemented as a simple function of average power based on (1) [13]. The isothermal drain current in (1) is given by

$$i_{D(T_o)} = \frac{B}{1+vs^{\Gamma}}\left[vs^{Q} - \left(\mathcal{M}\left(v_D, \frac{vs}{vs+\xi}\right)\right)^{Q}\right] \quad (3)$$

$$v_s = \sigma \ln\left[1+\exp\frac{v_{GS}-\gamma v_{GD}-V_{TO}}{\sigma}\right] \quad (4)$$

$$v_D = \sigma \ln\left[1+\exp\frac{v_{GD}-\gamma v_{GS}-V_{TO})}{\sigma}\right] \quad (5)$$

where Γ, Q, σ, and ξ are model parameters, and the function $\mathcal{M}()$ smoothly implements the saturation knee at low drain–source potentials. Equations (4) and (5) give positive-valued effective depletion potentials at the source and drain ends of the channel, respectively. Nonthermal dispersion is described by giving bias dependence to the transconductance scaling factor, β, pinchoff potential, V_{TO}, and drain–feedback term γ.

The time evolution of the dispersion effects is described by the process used to calculate the time-averaged terminal potentials and power dissipation. In the simplest form, which is adequate for most applications, a single time constant is used in determining the averages. Thus, the model keeps track of time in terms of average values of the voltages and power. The time constants are chosen to best approximate the transient behavior such as shown Fig. 4. A more elaborate model can be constructed by using multiple time constants to describe the series of thermal paths from junction to ambient. Bias-dependent time constants would better describe the effects of impact ionization.

The extraction of the model parameters is illustrated in the following example. Instantaneous *I/V* characteristics of a 400-μm pseudomorphic high electron-mobility transistor (pHEMT) were measured with 300-ns pulses for a range of initial operating points (in this example, 20). The parameters for the above model were extracted from the pulse data at each initial point by a simplex-based least-squares optimal fitting of the model to the data. The variation of the key parameters, pinchoff potential V_{TO}, gain β, and drain–feedback factor γ is described as polynomial functions fitted to their variation with bias. Fig. 5 shows the fitted variation of these parameters. The gain parameter β is seen to be of primary importance for describing the observable dispersion.

Given a bias condition, the corresponding values of the model parameters describe the pulse characteristics at that bias. The overall model tracks the changes in bias as a function of time and adjusts the model parameters accordingly. That is, the model parameters are functions of $\overline{V_{GS}}$ and $\overline{V_{GD}}$ and $\overline{I_{DS}V_{DS}}$. During a transient simulation, the bias is calculated as an average accumulated over time constants chosen to fit the dispersion rates. This adjustment of the key parameters as a function of bias gives an accurate simulation of the transient response, which is illustrated in Fig. 6 for the extracted device. The transients shown exhibit *drain overshoot* and *gate–lag* effects, which the model is able to simulate. The initial rise shown in this figure at around 10 μs is due to impact ionization dispersion, and the later change at around 100 μs is due to the thermal dispersion.

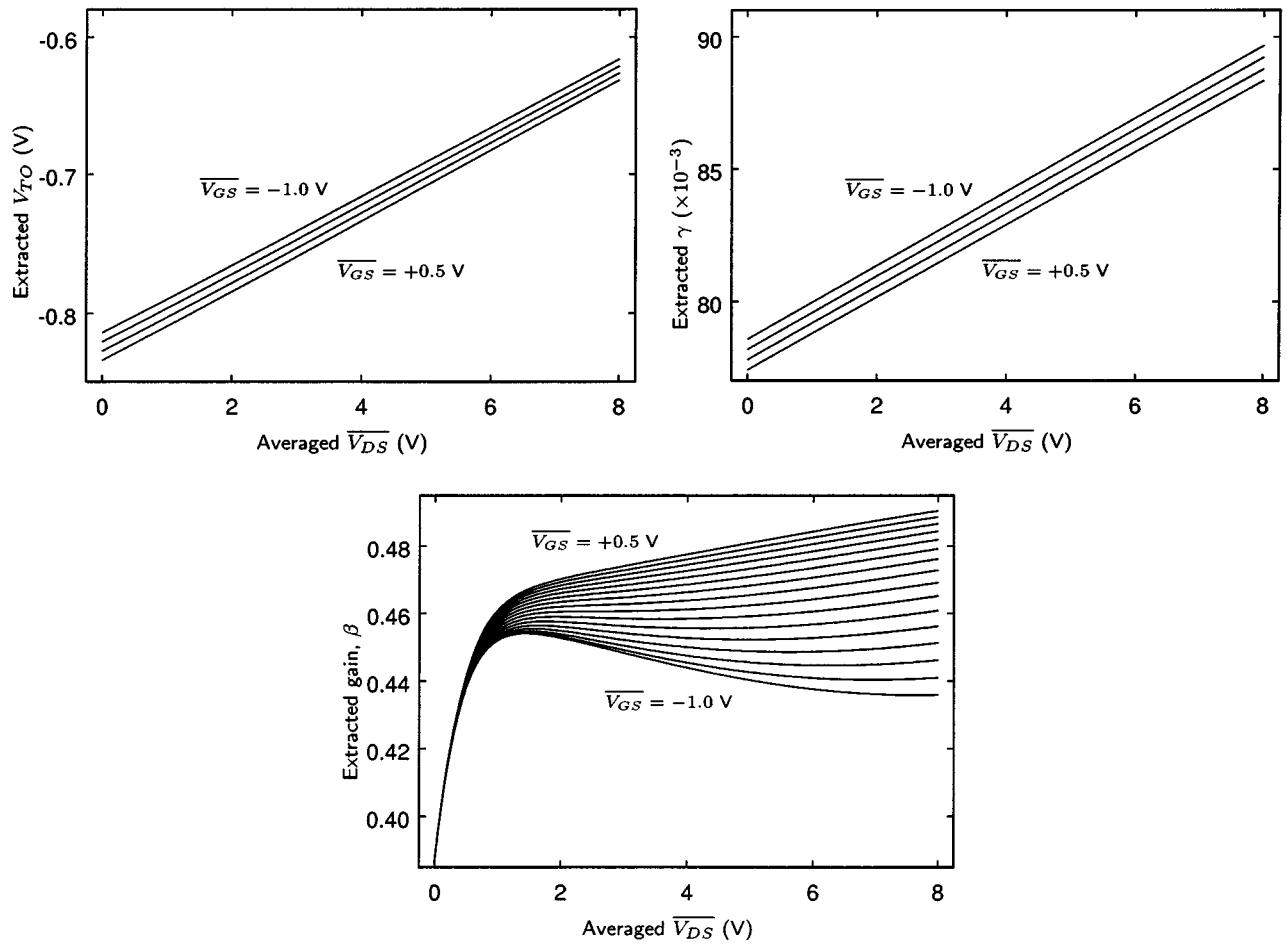

Fig. 5. Extracted model parameters versus average drain potential $\overline{V_{DS}}$ with gate bias as the parameter.

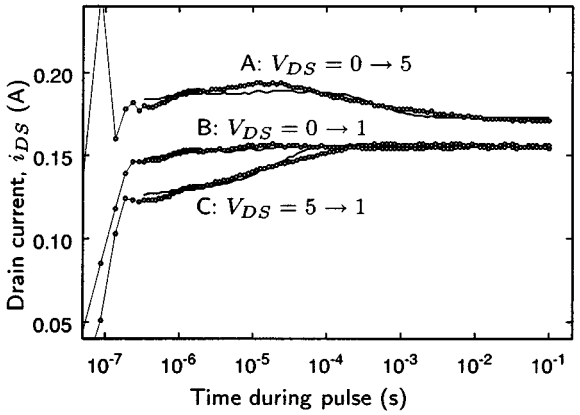

Fig. 6. Measured (∘) and simulated (—) drain–current response to pulses. In all cases, the gate voltage is pulsing from an initial operating point of $V_{GS} = -1$ V to a value of 0.0 V and the annotations give the drain voltage step.

V. Conclusion

A clear view of the dynamics of the dispersion effects in an HEMT has been shown as an evolution over time of its pulsed characteristics to its dc characteristics. The dynamics involved in this transition can be explained, for the most part, in terms of self-heating and charge-trapping related to impact ionization currents.

A simple modeling strategy has been presented to describe the observed transient behavior of an HEMT. This model gives bias dependence to the characteristics and tracks the changes in bias so that the time evolution of the characteristics is described. This examination of HEMT large-signal behavior provides a better perspective for understanding the dynamics involved and an insight and grounding for future work.

References

[1] J. B. Scott, J. G. Rathmell, A. E. Parker, and M. M. Sayed, "Pulsed device measurements and applications," *IEEE Trans. Microwave Theory Tech.*, vol. 44, pp. 2718–2723, Dec. 1996.

[2] A. E. Parker, J. Rathmell, and J. Scott, "Pulsed measurements," in *The Modern Microwave and RF Handbook*, M. Golio, Ed. Boca Raton, FL: CRC Press, 2000, ch. 4.1, pp. 4-68–4-95.

[3] P. H. Ladbrooke and S. R. Blight, "Low-field low-frequency dispersion of transconductance in GaAs MESFET's with implications for other rate-dependent anomalies," *IEEE Trans. Electron Devices*, vol. 35, pp. 257–267, Mar. 1998.

[4] W. Kruppa and J. B. Brad, "Low-frequency transconductance dispersion in In-AlAs/InGaAs/InP HEMT's with single- and double-recessed gate structures," *IEEE Trans. Electron Devices*, vol. 44, p. 687, May 1997.

[5] F. Filicori, G. Vannini, A. Santerelli, A. Mediavilla, A. Tazon, and Y. Newport, "Empirical modeling of low frequency dispersive effects due to traps and thermal phenomena in III–V FET's," *IEEE Trans. Microwave Theory Tech.*, vol. 43, pp. 2972–2982, Dec. 1995.

[6] A. N. Ernst, M. H. Somerville, and J. A. del Alamo, "Dynamics of the kink effect in In-AlAs/InGA's HEMT's," *IEEE Electron Device Lett.*, vol. 18, pp. 613–615, Dec. 1995.

[7] D. E. Root, "Foundations of measurement-based modeling for nonlinear circuit simulations," presented at the IEEE MTT-S New Directions Nonlinear RF Microwave Characterization Workshop, June 1996.
[8] A. E. Parker and D. E. Root, "Pulse measurements quantify dispersion in PHEMT's," in *URSI Signals, Syst., Electron. Symp.*, Sept. 29–Oct. 2, 1998, pp. 444–449.
[9] T. Suemitsu, T. Enoki, N. Sano, M. Tomizawa, and Y. Ishii, "An analysis of the kink phenomena in In-AlAs/InGaAs HEMT's using two-dimensional device simulation," *IEEE Trans. Electron Devices*, vol. 45, pp. 2390–2399, Dec. 1998.
[10] M. H. Somerville, A. Ernst, and J. A. del Almo, "A physical Model for the kink effect in In-AlAs/InGaAs HEMT's," *IEEE Trans. Electron Devices*, vol. 47, pp. 922–930, May 2000.
[11] R. T. Webster, S. Wu, and A. F. M. Anwar, "Impact ionization in InAlAs/InGaAs/InAlAs HEMT's," *IEEE Electron Device Lett.*, vol. 21, pp. 193–195, May 2000.
[12] A. E. Parker and D. J. Skellern, "A realistic large-signal MESFET model for SPICE," *IEEE Trans. Microwave Theory Tech.*, vol. 45, pp. 1563–1571, Sept. 1997.
[13] A. E. Parker, "Implementing SPICE models with high-order continuity and rate dependence," *Proc. Inst. Elect. Eng.*, pt. G, vol. 141, pp. 251–257, Aug 1994.

Anthony E. Parker (S'84–M'84–SM'95) received the B.S., B.E., and Ph.D. degrees from The University of Sydney, Sydney, N.S.W., Australia, in 1983, 1985, and 1992, respectively.

In 1993, he began his involvement with VHF radio and microwave systems, and satellite Earth-station installations. In 1986, he began research in design techniques and circuit models for gallium–arsenide microwave technology at The University of Sydney. This was in collaboration with the Division of Radiophysics, Commonwealth Scientific and Industrial Research Organization (CSIRO). In 1990, he joined Macquarie University, Sydney, N.S.W., Australia, where he is currently an Associate Professor and Head of the Electronics Department. He is currently involved with the project on pulsed characterization of microwave devices and design of low-distortion communications circuits. He has been a consultant and Visiting Scientist with several companies, including Microwave Semiconductor Division, M/A-COM, Lowell, MA, and Agilient Technologies, Santa Rosa, CA. He has developed accurate circuit simulation techniques, such as used in the Parker–Skellern FET model now installed in commercial simulators. He continues to develop a pulsed-bias and pulsed S-parameter characterization system within the Collaborative Nonlinear Electronics Research Facility at Macquarie University. He has authored or co-authored over 90 publications.

A/Prof. Parker is a member of the Institution of Telecommunications and Electronic Engineers, Australia. He has served on the Technical Committees for the 2000 IEEE Asia–Pacific Microwave Conference, Sydney, Australia and was the technical co-chair of the 2001 IEEE Symposium on Circuits and Systems, Sydney, Australia.

James Grantley Rathmell (M'89) was born in Australia, in 1955. He received the B.S., B.E., and Ph.D. degrees from The University of Sydney, Sydney, N.S.W., Australia, in 1977, 1979, and 1988, respectively.

From 1979 to 1981, he was involved with radio astronomy with both the Molonglo and Fleurs aperture synthesis telescopes. Under these programs, he was involved with signal and image analysis and the design of various microprocessor-based control hardware and software. From 1982 to 1986, he was involved with gate-array and very large-scale integration (VLSI) design of digital integrated circuits, principally for communications, and researched the behavioral modeling of digital circuits. During this time, he was a member of the teaching staff at The University of Sydney. In 1986, he joined The Nucleus Group, where he was involved with the design of biomedical equipment and managed the research and development of advanced ultrasound imaging equipment. In 1989, he returned to The University of Sydney, where he is currently a Senior Lecturer in digital systems. During this time, he has been involved with fiber-optic video-conferencing and digital audio signal processing. In 1995, he collaborated with Macquarie University on the development of pulsed-bias and pulsed S-parameter characterization of microwave devices. His main contribution in this area has been in signal-processing algorithms and measurement control software.

Dr. Rathmell served on the Technical and Local Arrangements Committees for the 2001 IEEE Symposium on Circuits and Systems, Sydney, N.S.W., Australia.